Available online at www.sciencedirect.com
SCIENCE DIRECT®
International Journal of Heat and Fluid Flow 27 (2006) 619–626
International Journal of HEAT AND FLUID FLOW
www.elsevier.com/locate/ijhff

LES–DPS of the effect of wall roughness on dispersed-phase transport in particle-laden turbulent channel flow

Kyle D. Squires [a,*], Olivier Simonin [b]

[a] Department of Mechanical and Aerospace Engineering, Arizona State University, Tempe, AZ 85287, USA
[b] Institut de Mécanique des Fluides, UMR 5502 CNRS/INPT/UPS, Allée du Professeur Camille Soula, 31400 Toulouse, France

Available online 27 March 2006

Abstract

The influence of wall roughness on dispersed-phase properties of particle-laden turbulent channel flow is investigated using large eddy simulation (LES) for the fluid flow and discrete particle simulation (DPS) for the particulate phase. Gas–solid flows are considered for which the particle equation of motion includes the contribution from the drag force. The influence of wall roughness is treated stochastically in which the impact angle is comprised of the particle trajectory angle and a stochastic component due to wall roughness. Elastic particle–wall collisions are considered with surface roughness characterized in terms of the standard deviation of the distribution of wall roughness angles. Computations are performed for three Stokes numbers and standard deviations in the wall roughness angle of 0 (smooth wall), 2.5° and 5°. LES–DPS results show that for a given wall roughness angle and particle Stokes number the most pronounced effect is on the wall-normal component of the particle velocity, which can be substantially increased by roughness. While the streamwise particle velocity variance also increases, the spanwise particle fluctuating velocity exhibits relatively little sensitivity to surface roughness. In addition, LES/DPS results show that wall roughness increases turbulent transport of the wall-normal particle velocity variance, in turn providing a mechanism for elevation of the particle velocity fluctuations across the entire flow.

Keywords: Particle-laden turbulent flow; Wall roughness

1. Introduction

Turbulent gas flows containing dilute suspensions of solid particles are complex and pose many technologically challenging and scientifically relevant questions. For the practical applications in which particle-laden turbulent flows are encountered, statistical models that require empirical input will continue to form the basis for engineering prediction. The fundamental knowledge base that is crucial for guiding the development of models for applications is not, however, sufficiently developed. This is in large part due to the difficulty in measuring quantities in the reference frame most naturally suited for analysis, i.e., the Lagrangian reference frame attached to a particle. This complicates experiments and motivates the application of numerical simulations that enable detailed investigation of many of the processes governing turbulent two-phase flows.

For dilute, gas–solid turbulent flows, numerical techniques that resolve some or all of the underlying eddy motions of the carrier-phase have an important role in advancing fundamental understanding of the various interactions important to accurately predicting dispersed-phase properties. These numerical approaches – direct numerical simulation (DNS) and large eddy simulation (LES) – together with discrete particle simulation (DPS) have been applied in several previous investigations aimed at understanding particle transport by turbulence, particle–particle collisions, and turbulence modulation by momentum exchange with heavy particles (e.g., see Laviéville et al., 1995; Wang and Squires, 1996; Boivin et al., 1998; Yamamoto et al., 2001).

* Corresponding author.
E-mail addresses: squires@asu.edu (K.D. Squires), simonin@imft.fr (O. Simonin).

0142-727X/$ - see front matter © 2006 Elsevier Inc. All rights reserved.
doi:10.1016/j.ijheatfluidflow.2006.02.009

These and other works have been useful for exploring fundamental aspects of gas–solid turbulent flows through controlled, parametric studies. The capacity to precisely define and control the parameter space is useful since the presence of a dispersed phase of heavy particles introduces several additional parameters over those already relevant to characterizing single-phase turbulence. The relevant timescales include the particle response time, the inter-particle collision time, and for wall-bounded flows the timescale characterizing particle–wall collisions. Comparison against the appropriate fluid flow timescales has generally been thought to indicate the relative importance of a given effect, though it is increasingly clear in multiphase flows in general, and gas–solid turbulent flows in particular, that it is not possible to develop simple criteria that would accurately indicate the dominance of a particular effect.

Less investigated than the effects cited above using techniques such as DNS and LES, and the topic of the present effort, is the influence of wall roughness on particulate-phase transport. Experimental investigations have shown that wall roughness can strongly alter particle motion and in turn cause measurable changes to the overall flow properties. Sommerfeld and Huber (1999) showed that wall roughness altered the rebound behavior of particles in a horizontal channel flow which, on average, resulted in a re-dispersion of the particles as well as a lowering of the settling rate as compared to measurements in smooth-wall configurations. Kussin and Sommerfeld (2002) obtained measurements of gas–solid, horizontal channel flow using spherical beads with diameters ranging from 60 μm to 1 mm. A focus of that work was variation of wall roughness by changing the wall plates. Their measurements showed that wall roughness enhanced the particle fluctuating velocity due to the irregular bouncing of the particle with a rough wall and lead to a more uniform distribution of particles across the channel.

In general, measurements show that wall roughness introduces an effect analogous to that produced by particle–particle collisions: amplification of wall-normal (or, in a pipe, radial) particle velocity fluctuations that can substantially change the transport characteristics of the particles and cause large changes in other flow properties, e.g., the overall pressure drop of a gas–solid mixture. Sommerfeld and Huber (1999) used their experiments to measure parameters for a wall-collision model employed in Lagrangian approaches for gas-particle flows as described in Sommerfeld (1992) (see also Sommerfeld, 2003). As described below, a similar approach to incorporating the effect of wall roughness into the computations is employed in the present study. The reader is further referred to Tsuji et al. (1987), Sakiz and Simonin (1999), and Zhang and Zhou (2004) for additional discussion and background of related approaches to modeling particle–wall collisions.

As summarized in the next section, the computational approach is based on LES of fully-developed turbulent channel flow combined with discrete particle simulation (DPS) of the dispersed phase. The particle equation of motion and parameter space of the present investigations are presented and followed by statistical descriptors of particulate-phase motion used to assess roughness effects. A summary of the work and perspectives gained are then outlined.

2. Approach

2.1. LES of turbulent channel flow

The flow under consideration is a vertical, fully-developed turbulent channel flow (i.e., without gravitational settling on either of the channel walls). The numerical approach employs large eddy simulation (LES) of the carrier-phase flow and discrete particle simulation (DPS) for prediction of dispersed phase transport. The fluid flow is maintained at constant mass flux corresponding to a target Reynolds number $Re_\tau = 180$ based on the friction velocity u_τ and channel halfwidth δ. The dimensions of the channel are $4\pi\delta$ in the streamwise (x or x_1), $4\pi\delta/3$ in the spanwise (z or x_3), and 2δ in the wall-normal (y or x_2) directions. Periodic boundary conditions are applied to the dependent variables in the streamwise and spanwise dimensions and no-slip boundary conditions to the velocity at the channel walls. The subgrid-scale stress arising from the filtering of the Navier–Stokes equations is closed using the eddy viscosity model of Piomelli et al. (1989).

The equations governing the fluid flow are solved using a fractional step method (e.g., see Burton and Eaton, 2002) on a staggered mesh comprised of $64 \times 64 \times 64$ cells in the x, y, and z directions, respectively. The grid spacings in the streamwise and spanwise directions are uniform with corresponding spacings in viscous units of $\Delta x^+ = 35$ and $\Delta z^+ = 12$. Spatial derivatives are approximated using second-order accurate central differences. The Poisson equation formulated for the pressure variable that is used to obtain a divergence-free velocity field is solved using fast transforms in the streamwise and spanwise direction, resulting in a series of tri-diagonal matrices that are efficiently inverted in the direction normal to the solid walls. The wall-normal mesh is clustered near the solid surfaces and stretched away from the wall using a hyperbolic tangent function. The discretized system is advanced in time using an implicit/explicit time advance (Crank–Nicholson and second-order Adams–Bashforth).

2.2. Discrete particle simulation

The focus of the current work is on dilute gas–solid flows in the limit of one-way coupling (i.e., no modification of the carrier phase flow due to momentum exchange with the dispersed phase) and without inter-particle collisions. The particle density is much larger than that of the fluid phase, ($\rho_p \gg \rho_f$, where ρ_f is the fluid density and the ρ_p is the particle density). Owing to the large density ratio, the particle response time is large compared to the Kolmogorov timescale of the undisturbed flow.

For the dilute regimes under consideration, the force induced by the surrounding fluid flow on the particles reduces to the drag. The equation of motion for a single particle is written as

$$\frac{\mathrm{d}v_{\mathrm{p},i}}{\mathrm{d}t} = -\frac{3}{4}\frac{\rho_{\mathrm{f}}}{\rho_{\mathrm{p}}}\frac{C_{\mathrm{D}}}{d_{\mathrm{p}}}|v_{\mathrm{r}}|v_{\mathrm{r},i}, \tag{1}$$

where the particle diameter d_{p} is of the same order or smaller than the smallest length scales in the carrier flow, $v_{\mathrm{p},i}$ is the ith component of the particle velocity, and $v_{\mathrm{r},i}$ is the particle relative velocity,

$$v_{\mathrm{r},i} = v_{\mathrm{p},i} - \widetilde{u}_{\mathrm{f},i}, \tag{2}$$

$$C_{\mathrm{D}} = \frac{24}{Re_{\mathrm{p}}}(1 + 0.15Re_{\mathrm{p}}^{0.687}), \quad Re_{\mathrm{p}} = \frac{|v_{\mathrm{r}}|d_{\mathrm{p}}}{v_{\mathrm{f}}}, \tag{3}$$

where the kinematic viscosity of the fluid is denoted v_{f} and $\widetilde{u}_{\mathrm{f},i}$ is the locally undisturbed fluid velocity at the particle position. As also shown in (3), the correlation for the drag coefficient from Schiller and Nauman (1935) is introduced to extend the Reynolds number range of the drag force.

Simulations are performed for three particle Stokes numbers, $St = 0.1625$, 0.65, and 2.60 where $St = \tau_{\mathrm{ps}}/(\delta/u_\tau)$ and τ_{ps} is the Stokes relaxation time of the particle. For all simulations the particle diameter was specified as one viscous unit and therefore the variation in the Stokes number is achieved by changing the density ratio. The particle response times span a relatively wide range, from the smallest value $St = 0.1625$ that characterize particles which follow much of the turbulent fluctuations in the carrier phase while for the largest $St = 2.60$ the particles are substantially unresponsive to the carrier-phase turbulent flow.

Properties of the dispersed phase are obtained via Lagrangian tracking of 1×10^5 particles, corresponding to an average number density of 950 particles per unit volume (i.e., the entire ensemble of 10^5 particles normalized by the volume of the channel). The particle equation of motion (1) is integrated in time using second-order Adams–Bashforth. Fourth-order Lagrange polynomials are used to interpolate the fluid velocity to the particle position. Particle displacements are also integrated using the second-order Adams–Bashforth method. For particles that move out of the channel in the streamwise or spanwise directions, periodic boundary conditions are used to reintroduce them into the computational domain.

In this work, the fluid flow is not influenced by momentum exchange with the particles and the undisturbed fluid velocity $\tilde{u}_{\mathrm{f},i}$, required in (2), is the value interpolated to the particle position that is computed in the LES, representing the spatially-filtered (volume averaged) solution of the Navier–Stokes equations. The influence of subgrid-scale transport on particle motion is not considered, which should be a reasonable assumption given the filtering by particle inertia of the smaller-scale, high-frequency components of the subgrid fluid velocity (e.g., see Yamamoto et al., 2001). However, the neglect of subgrid transport restricts the parameter range of the current calculations, e.g., to lower Reynolds numbers in which it is not difficult to resolve the vast majority of the turbulence kinetic energy using the grid resolutions applied in this work. The unresolved component of the kinetic energy is then a very small fraction of the total and, coupled with the filtering effect of particle inertia, the influence of subgrid-scale velocity fluctuations on particle motion will not be strong. In other regimes, such as very small particle response times, the errors introduced by transporting the particulate phase by a filtered fluid velocity should be significant and will require models of the subgrid velocities on particle motion.

Particles collide with a "virtual wall" which has a randomly distributed inclination with respect to the plane, smooth wall where the "wall roughness angle" is denoted γ in the plane shown in Fig. 1. The stochastic treatment is similar to that employed in Sommerfeld (2003) (and related references therein). Three values of the standard deviation, $\Delta\gamma$, of the distribution of wall roughness angles are considered: 0° (smooth wall), 2.5° and 5°. These values are within the range of the measurements from Sommerfeld and Huber (1999) used to develop and validate roughness models for Lagrangian approaches.

In the LES/DPS calculations performed in the current work that are three-dimensional the "virtual wall" is defined by the surface normal

$$n = [\sin\phi\cos\theta, \cos\phi, \sin\phi\sin\theta], \tag{4}$$

where the angles ϕ and θ are obtained from Gaussian distributions (note that $\phi = \theta = 0°$ corresponds to the smooth wall with the normal vector aligned with the wall-normal y-coordinate). Denoting the incident (i.e., toward the wall) particle velocity as v_{p}^- and the reflected particle velocity as v_{p}^+, then the relation between the reflected velocity and incident values are

$$v_{\mathrm{p}}^+ = v_{\mathrm{p}}^- - 2(v_{\mathrm{p}}^- \cdot n)n. \tag{5}$$

Following sampling of the Gaussian distributions to obtain the random angles ϕ and θ, (5) is applied to determine the rebound velocity of the particle with the constraint that the wall-normal component be directed into the flow (with new angles sampled in the event that the rebound velocity was not towards the flow following a wall collision).

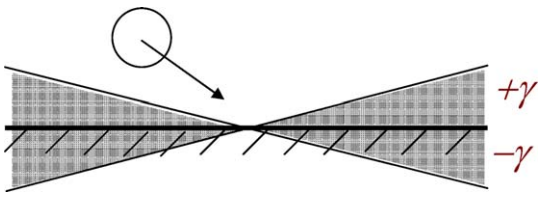

Fig. 1. Particle collision with a "virtual wall" in which particle collides with a wall given a random inclination. Wall roughness angles are sampled from a Gaussian distribution that is characterized by its standard deviation $\Delta\gamma$.

3. Results

3.1. Mean flow

Shown in Fig. 2 is the wall-normal profile of the mean particle number density, n_p, for each Stokes number and from a smooth-wall case ($\Delta\gamma = 0°$) and rough-wall case with $\Delta\gamma = 5°$. The figure shows that for particle–wall collisions with a smooth wall the number density exhibits a characteristic peak in the near-wall region as observed in channel flows in which particle–particle collisions are not considered and for which there is a specular reflection of the particle from the wall (e.g., see Yamamoto et al., 2001). As shown in the figure, the most significant non-uniformity in the wall-normal profiles for the smooth-wall cases is observed for the lower Stokes numbers, $St = 0.1625, 0.65$.

Fig. 2 shows that, compared to the smooth-wall profiles, for the rough wall case $\Delta\gamma = 5°$ the number density undergoes the largest changes for the largest Stokes number, $St = 2.60$. Note that the bulk concentrations for all of the cases are identical (the entire range of the number density very close to the wall is not shown in the figure to highlight the changes in the core of the flow). For the lightest particles, $St = 0.1625$, there are only minor changes between the profiles (and for other statistics not shown here). For $St = 0.65$ and $St = 2.60$ the influence of wall roughness becomes more apparent with Fig. 2 showing that the rough-wall profiles become more uniform and with the largest changes occurring close to the wall.

The effect of wall roughness on the mean streamwise particle velocity, $V_{p,1}$, is shown in Fig. 3 for $St = 0.65$ and $St = 2.60$ and for roughness angles of 0 and 2.5 degrees. Also shown in the figure is the profile of the mean

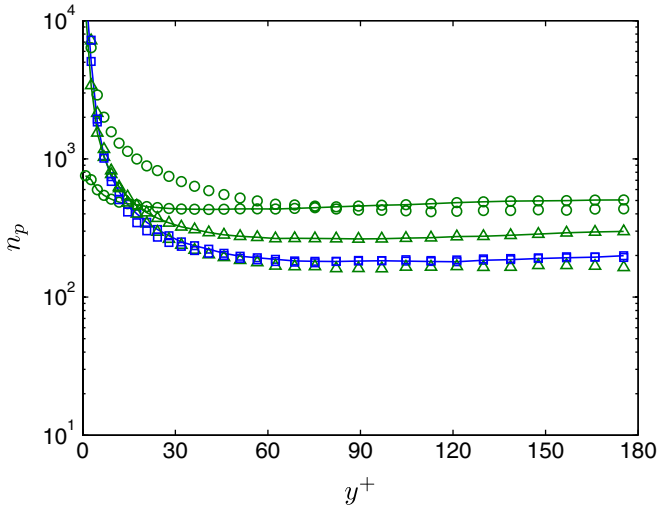

Fig. 2. Wall-normal profile of the mean number density (average number density over the entire particle ensemble and channel is 950 particles per unit volume). Rough-wall results with $\Delta\gamma = 5°$ shown using symbols and lines; smooth-wall ($\Delta\gamma = 0°$) cases shown using symbols only. (□) $St = 0.1625$; (△) $St = 0.65$; (○) $St = 2.60$.

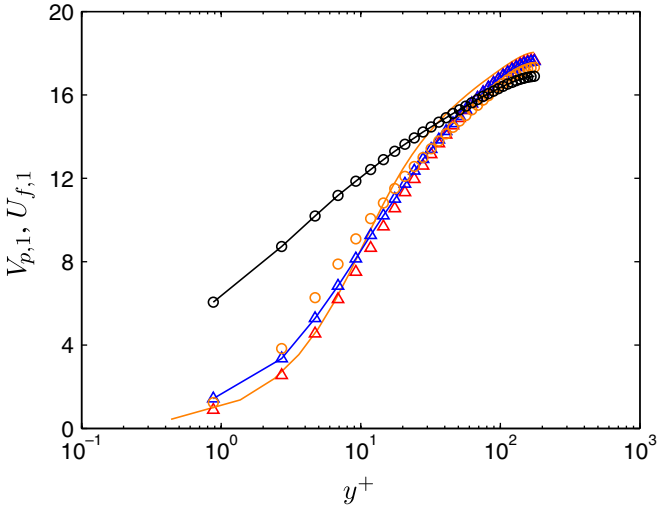

Fig. 3. Wall-normal profile of the mean streamwise mean velocity; all profiles are normalized by the friction velocity of the fluid, u_τ. Rough-wall results with $\Delta\gamma = 2.5°$ shown using symbols and lines; smooth-wall ($\Delta\gamma = 0°$) cases shown using symbols only. (—) fluid; (△) $St = 0.65$; (○) $St = 2.60$.

fluid velocity on the grid $U_{f,1}$, i.e., not along particle trajectories. Each of the profiles shown are normalized by the friction velocity of the fluid, u_τ and it is also noted that the mean velocities for both phases in the wall-normal and spanwise directions are zero. For the smooth-wall cases (symbols-only in the figure) the mean slip between the particles and fluid is small and, consequently, the mean velocity of the particles is close to that of the fluid. Analogous to the more uniform profiles achieved in the number density depicted in Fig. 2, for the rough-wall cases Fig. 3 shows that the particle mean velocity profile becomes more uniform across the channel. As shown in the figure, this effect is the most apparent for the largest Stokes number, $St = 2.60$, where the velocity is not only more uniform for the rough-wall case but also slips relative to the wall, which is compatible with the elastic bouncing of the particles as considered in the current simulations.

The mean number density and mean streamwise velocity in Figs. 2 and 3 show effects of wall roughness that appear comparable to those produced by inter-particle collisions in which the redistribution of particle kinetic energy by particle–particle collisions provides a mechanism for increasing cross-stream (wall-normal or radial) transport, and also leads to more uniform number density distributions and particle mean velocities.

3.2. Influence of wall roughness on the particle velocity variance

The influence of wall roughness on the particle velocity variance for $St = 0.65$ is shown in Figs. 4–6 for the streamwise, wall-normal, and spanwise directions, respectively. The profiles shown in these figures are representative of the other Stokes numbers not shown here. Plotted in each

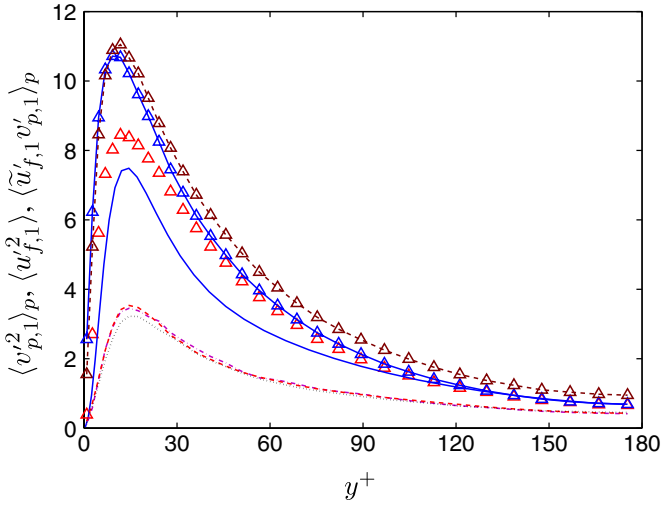

Fig. 4. Influence of roughness on streamwise velocity variance, $St = 0.65$; all profiles are normalized u_τ^2. (—) fluid; (△) smooth wall; (△—△) $\Delta\gamma = 2.5°$; (△- -△) $\Delta\gamma = 5°$; (– · –) fluid-particle correlation for smooth wall; (- - -) fluid-particle correlation for $\Delta\gamma = 2.5°$; (· · ·) fluid-particle correlation for $\Delta\gamma = 5°$.

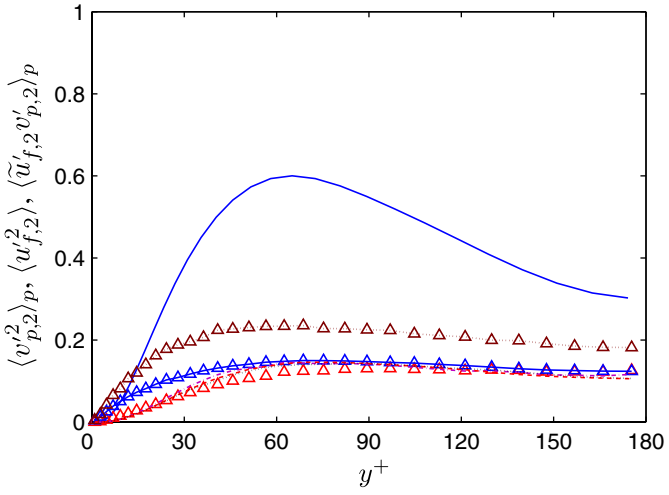

Fig. 5. Influence of roughness on wall-normal velocity variance, $St = 0.65$; all profiles are normalized by u_τ^2. (—) fluid; (△) smooth wall; (△—△) $\Delta\gamma = 2.5°$; (△···△) $\Delta\gamma = 5°$; (– · –) fluid-particle correlation for smooth wall; (- - -) fluid-particle correlation for $\Delta\gamma = 2.5°$; (· · ·) fluid-particle correlation for $\Delta\gamma = 5°$.

figure is the particle velocity variance for the three roughness angles, the fluid variance, and the fluid-particle velocity correlation, $\langle \tilde{u}'_{f,\alpha} v'_{p,\alpha}\rangle_p$ for each of the wall roughness cases. Note that $\langle\cdot\rangle_p$ denotes an average over the particulate phase in the statistically homogeneous wall-parallel planes and time; the velocity fluctuations are defined by subtracting the mean values from the corresponding instantaneous velocities. For the fluid, the fluctuating velocity following the particle is denoted $\tilde{u}'_{f,\alpha}$ while the fluid velocity fluctuation on the grid is denoted $u'_{f,\alpha}$(the average shown in the figure taken over the grid in x–z planes and time is represented using $\langle\cdot\rangle$).

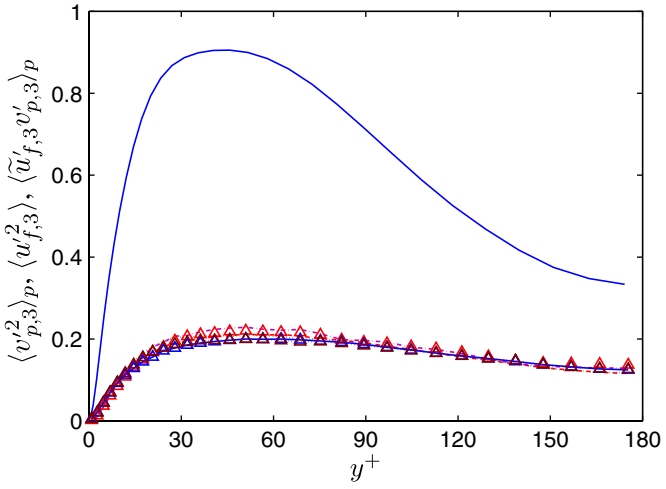

Fig. 6. Influence of roughness on spanwise velocity variance, $St = 0.65$; all profiles are normalized by u_τ^2. (—) fluid; (△) smooth wall; (△—△) $\Delta\gamma = 2.5°$; (△- -△) $\Delta\gamma = 5°$; (– · –) fluid-particle correlation for smooth wall; (- - -) fluid-particle correlation for $\Delta\gamma = 2.5°$; (· · ·) fluid-particle correlation for $\Delta\gamma = 5°$.

The general effects of wall roughness depicted in Figs. 4–6 are an increase of the wall-normal and streamwise particle velocity variance, with the largest effects of roughness on the wall-normal variance, and then with negligible effects of roughness on the spanwise variance. Fig. 4 shows that for the smooth-wall case ($\Delta\gamma = 0°$), the particle velocity fluctuations for $St = 0.65$ exceed the fluid levels near the wall and are also substantially larger than the fluid-particle velocity variance. As shown by Simonin et al. (1995) and Wang and Squires (1996), this feature arises due to the production of the streamwise particle velocity fluctuations by gradients in both the mean particle and mean fluid velocities with the particle velocity fluctuations possibly becoming larger than the corresponding value for the fluid, as shown in the figure. Fig. 4 shows that the streamwise particle velocity variance exhibits relatively little change with increases in the roughness angle from $\Delta\gamma = 2.5°$ to 5°, one contributor being a smaller gradient in the mean particle velocity with increasing roughness.

While the streamwise particle velocity variance is comparable (larger) than that for the fluid, Figs. 5 and 6 show that the wall-normal and spanwise velocity variances for the smooth-wall case ($\Delta\gamma = 0°$) are substantially smaller than that of the corresponding levels in the fluid. This is an intuitive effect of particle inertia which results in very large anisotropy of the particle velocity fluctuations in the smooth-wall case. Figs. 5 and 6 also show that the particle wall-normal and spanwise velocity variances are in good agreement with the corresponding profiles of the fluid-particle velocity correlations. As also discussed below, this is indicative that the the particle fluctuating motion in these directions is controlled by the drag force and that effects of turbulent dispersion (triple correlation transport) are not substantial. Thus, particle fluctuating motion in these directions is at equilibrium with the local turbulent fluid flow.

Fig. 5 also shows that for $\Delta\gamma = 2.5°$ the wall-normal particle velocity variance is tangibly larger than the smooth-wall profile in the near-wall region (for values of y^+ less than about 50) and slightly larger than the smooth-wall profile to approximately $y^+ = 100$. With further increases in roughness, to $\Delta\gamma = 5°$, Fig. 5 shows that the wall-normal particle velocity variance is larger than the smooth-wall profile throughout the channel, showing that the effects of roughness on the particle fluctuating motion have permeated throughout the flow. Though not large, in the very near wall region, for y^+ smaller than about 10, Fig. 5 shows that the particle variance is slightly larger than the fluid value. Also apparent from the figure is that the wall-normal particle velocity fluctuations are no longer at equilibrium with the local turbulent fluid flow, as evidenced by the discrepancy between the particle velocity variance and fluid-particle velocity correlation.

While Fig. 5 shows that there is a relatively large increase with roughness in the wall-normal particle velocity fluctuations, Fig. 4 shows that the streamwise velocity variance exhibits less sensitivity to increases in the roughness angle from 2.5° to 5°, indicative of a less efficient mechanism compared to that responsible for elevating the wall-normal particle velocity variance. As shown in Fig. 6, the influence of wall roughness on the spanwise particle velocity fluctuations is negligible with good agreement between the particle velocity variance and fluid-particle velocity correlation for all roughness angles. Also apparent in Figs. 4 and 5, while wall roughness can have strong effects on the particle velocity fluctuations, the fluid-particle correlations exhibit small changes.

3.3. Influence of Stokes number on the particle velocity variance

The effect of Stokes number on the particle velocity fluctuations for a fixed roughness angle is shown in Figs. 7–9. The results in these figures are for $\Delta\gamma = 2.5°$ and are representative of the effects observed for the larger angle $\Delta\gamma = 5°$. Analogous to Figs. 4–6, shown in Figs. 7–9 are the profiles of the fluid velocity variance on the grid and corresponding fluid-particle velocity correlations for each Stokes number.

Each of Figs. 7–9 shows that the fluid-particle velocity correlation decreases with increasing particle inertia and, as also observed previously for $St = 0.65$ in Figs. 5 and 6, the wall-normal and spanwise variances for $St = 2.60$ in Figs. 8 and 9 are in good agreement with the corresponding components of the fluid-particle velocity correlation for the smooth-wall case ($\Delta\gamma = 0°$).

Fig. 8 shows that the wall-normal particle velocity variance for $St = 2.60$ and $\Delta\gamma = 2.5°$ is larger than the curve for $St = 0.65$ and also substantially larger than the corresponding value of the fluid-particle velocity correlation (and therefore substantially above the particle velocity variance for the smooth-wall case). Fig. 8, which shows the wall-normal variance, illustrates that for $St = 2.60$ the

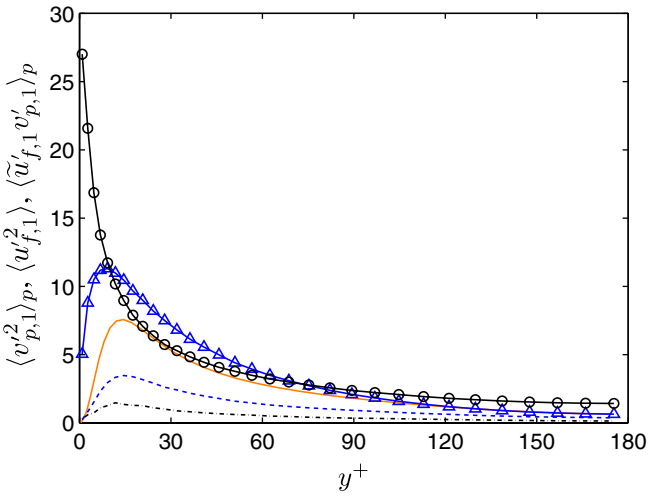

Fig. 7. Influence of Stokes number on the streamwise velocity variance, $\Delta\gamma = 2.5°$; all profiles are normalized by u_τ^2. (—) fluid; (▵—▵) $St = 0.65$; (○—○) $St = 2.60$; (- - -) fluid-particle correlation for $St = 0.65$; (– · –) fluid-particle correlation for $St = 2.60$.

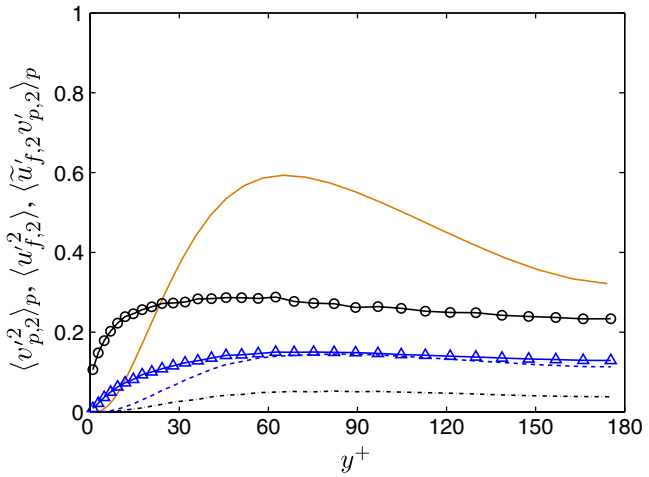

Fig. 8. Influence of Stokes number on the wall-normal velocity variance, $\Delta\gamma = 2.5°$; all profiles are normalized by u_τ^2. (—) fluid; (▵—▵) $St = 0.65$; (○—○) $St = 2.60$; (- - -) fluid-particle correlation for $St = 0.65$; (– · –) fluid-particle correlation for $St = 2.60$.

near-wall behavior is rather different than observed for $St = 0.65$, with a large increase in the variance at the wall. Fig. 9 shows that the spanwise variance for $St = 2.60$ is essentially unchanged (except very close to the wall) by wall roughness, indicating that the spanwise particle velocity fluctuations continue to be in equilibrium with the gas-phase turbulence throughout most of the flow.

3.4. Turbulent transport

Figs. 4–9 show that the largest effects on the particle fluctuating velocity occur in the wall-normal component and that for either increasing roughness or increasing Stokes number the velocity variance can be amplified throughout the channel, not only in the near-wall region

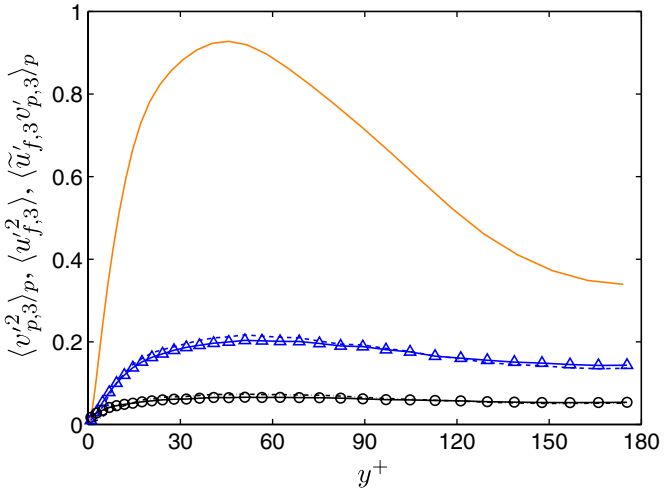

Fig. 9. Influence of Stokes number on the spanwise velocity variance, $\Delta\gamma = 2.5°$; all profiles are normalized by u_τ^2. (—) fluid; (▵—▵) $St = 0.65$; (○—○) $St = 2.60$; (- - -) fluid-particle correlation for $St = 0.65$; (– · –) fluid-particle correlation for $St = 2.60$.

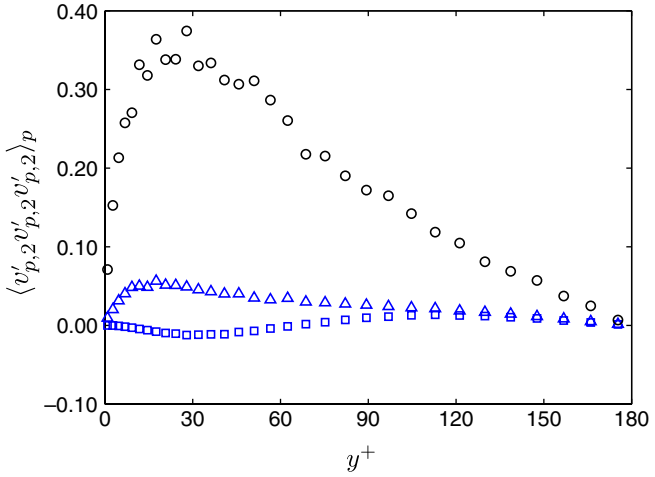

Fig. 10. Influence of roughness on turbulent transport of the wall-normal particle velocity variance by the wall-normal particle velocity, $\langle v'_{p,2}v'_{p,2}v'_{p,2}\rangle_p$, $St = 0.65$; all profiles are normalized by u_τ^3. (□) $\Delta\gamma = 0°$; (△) $\Delta\gamma = 2.5°$; (○) $\Delta\gamma = 5°$.

where effects of surface roughness would be anticipated. Insight into this feature is possible via examination of the transport equation for the particle velocity variance, which can be derived from the particle probability density function as shown in Simonin (2000) (see also Wang et al., 1998). For the wall-normal variance the transport equation can be written as

$$\left[\frac{\partial}{\partial t} + V_{p,2}\frac{\partial}{\partial x_2}\right]\langle v'_{p,2}v'_{p,2}\rangle_p = -\frac{1}{n_p}\frac{\partial}{\partial x_2}\left[n_p\langle v'_{p,2}v'_{p,2}v'_{p,2}\rangle_p\right] - \frac{2}{\tau^F_{fp}}\left[\langle v'_{p,2}v'_{p,2}\rangle_p - \langle \widetilde{u}'_{f,2}v'_{p,2}\rangle_p\right], \quad (6)$$

where τ^F_{fp} is an averaged particle relaxation time,

$$\frac{1}{\tau^F_{fp}} = \frac{3}{4}\frac{\rho_f}{\rho_p}\frac{C_D(\langle Re_p\rangle_p)}{d_p}\langle|v_p - \widetilde{u}_f|\rangle_p. \quad (7)$$

In the fully-developed turbulent channel flow as considered in this work the left-hand side of (6) is zero (because the statistics are time-independent and the particle wall-normal mean velocity $V_{p,2}$ is zero). The first term on the right-hand side represents the transport of the velocity variance by the wall-normal particle fluctuating velocity. The remaining terms on the right-hand side of (6) account for the interaction of the particles with the fluid turbulent motion. For cases in which the triple correlation term is negligible, (6) shows that there is then an equivalence between $\langle v'_{p,2}v'_{p,2}\rangle_p$ and $\langle \widetilde{u}'_{f,2}v'_{p,2}\rangle_p$. As already shown in Fig. 5 for the smooth-wall cases the particle velocity variance and corresponding component of the fluid-particle velocity correlation are in good agreement, consistent with a weak contribution of the triple correlation term. For the rough-wall cases, on the other hand, Figs. 5 and 8 show that the wall-normal particle velocity fluctuations increase while the fluid-particle velocity correlation is essentially unchanged. Eq. (6) shows that the increase in the wall-normal particle velocity variance compared to the fluid-particle correlation implies a more substantial role for the transport term.

Fig. 10 shows the effect of wall roughness on $\langle v'_{p,2}v'_{p,2}v'_{p,2}\rangle_p$ for $St = 0.65$. For the smooth-wall case, $\Delta\gamma = 0°$, the triple correlation is small, which is anticipated given (6) and the good agreement shown previously between the particle wall-normal velocity fluctuations and fluid-particle velocity correlation. Fig. 10 also shows that with increases in the roughness angle there is a significant increase in $\langle v'_{p,2}v'_{p,2}v'_{p,2}\rangle_p$ with the increase from the wall to a peak value and the decrease to the core of the channel indicative of a transport of the wall-normal particle velocity variance from the near-wall region to the channel core.

4. Summary and perspectives

The present effort focused on the influence of wall roughness on the transport characteristics of heavy particles in a gas–solid turbulent channel flow. The motion of the particles was dictated by their interactions with the local turbulent fluid flow and wall collisions. The smooth-wall cases show the effects characteristic of turbulent channel flow in the absence of particle–particle collisions or surface roughness, e.g., a peak in the near-wall particle number density and strong anisotropy of the particle velocity fluctuations. LES–DPS results for the smooth-wall case show the particle fluctuating motion in the wall-normal and spanwise directions is at equilibrium with the local turbulent fluid flow. The current simulations show that surface roughness results in the mean number density becoming more uniform and that the mean streamwise velocity of the particles also increases near the wall.

In general, while it would be anticipated that wall roughness will lead to direct changes to the particle veloc-

ities in the very near wall region, particle collisions with roughened surfaces can also enhance dispersed-phase transport across the entire channel. Examination of the triple velocity correlation representing the wall-normal transport of the wall-normal particle velocity fluctuations shows large changes with increasing roughness and that turbulent transport provides a mechanism for elevating velocity fluctuations across the flow, especially for the larger Stokes numbers and/or larger roughness angles.

For the particle fluctuating motion, wall roughness disrupts the equilibrium between the particle velocity fluctuations and gas-phase turbulent flow in the wall-normal direction, but nearly negligibly along the spanwise coordinate. LES–DPS results showed that the spanwise particle velocity variance was nearly unchanged from the smooth-wall result in cases with wall roughness. The small changes in the spanwise velocity fluctuations, while surprising, are consistent with pdf-based modeling approaches under development for Euler–Euler simulation techniques which also predict a weaker sensitivity of the spanwise fluctuating velocities to wall roughness. Further, pdf-based models show that the different responses of the particle fluctuating velocities to roughness arises due to different mechanisms. The current findings and models under development motivate further studies aimed at isolating the physical mechanisms governing roughness effects in addition to detailed assessment of engineering models.

Acknowledgements

The first author gratefully acknowledges the financial support of the Centre National de la Recherche Scientifique (CNRS) and Institut National Polytechnique de Toulouse (INPT).

References

Boivin, M., Simonin, O., Squires, K.D., 1998. Direct numerical simulation of turbulence modulation by particles in isotropic turbulence. J. Fluid Mech. 375, 235–263.

Burton, T.M., Eaton, J.K., 2002. Analysis of a fractional-step method on overset grids. J. Comp. Phys. 177, 336–364.

Kussin, J., Sommerfeld, M., 2002. Experimental studies on particle behavior and turbulence modification in horizontal channel flow with different wall roughness. Exp. Fluids 33, 143–159.

Laviéville, J., Simonin, O., Deutsch, E., 1995. Large Eddy Simulation of interactions between colliding particles and a homogeneous isotropic turbulence field. In: Gas–Solid Flows, ASME FED, vol. 228, pp. 347–357.

Piomelli, U., Ferziger, J.H., Moin, P., Kim, J., 1989. New approximate boundary conditions for large eddy simulation of wall-bounded flows. Phys. Fluid A 1, 1061–1068.

Sakiz, M., Simonin, O., 1999. Development and validation of continuum particle wall boundary conditions using Lagrangian simulation of a vertical gas–solid channel flow. FEDSM99-7898.

Schiller, L., Nauman, A., 1935. A Drag Coefficient Correlation. V.D.I. Zeitung 77, 318–320.

Simonin, O., Deutsch, E., Boivin, M., 1995. Large eddy simulation and second-moment closure model of particle fluctuating motion in two-phase turbulent shear flows. In: Durst, F., Kasagi, N., Launder, B.E., Schmidt, F.W., Whitelaw, J.H. (Eds.), Turbulent Shear Flow 9. Springer-Verlag, Heidelberg, pp. 85–115.

Simonin, O. 2000. Statistical and Continuum Modelling of Turbulent Reactive Particulate Flows. Part 1: Theoretical Derivation of Dispersed Eulerian Modelling from Probability Density Function Kinetic Equation'', in Theoretical and Experimental Modeling of Particulate Flows, Lecture Series 2000-06, von Karman Institute for Fluid Dynamics, Rhode Saint Genèse (Belgium).

Sommerfeld, M., 1992. Modelling of particle-wall collisions in confined gas-particle flows. Int. J. Multiphase Flow 18, 905–926.

Sommerfeld, M., Huber, N., 1999. Experimental analysis and modelling of particle-wall collisions. Int. J. Multiphase Flow 25, 1457–1489.

Sommerfeld, M., 2003. Analysis of collision effects for turbulent gas-particle flow in a horizontal channel: Part I. Particle transport. Int. J. Multiphase Flow 29, 675–699.

Tsuji, Y., Morikawa, Y., Tanaka, T., Nakatsukasa, N., Nakatani, M., 1987. Numerical simulation of pneumatic conveying in horizontal pipe. Int. J. Multiphase Flow 13.

Wang, Q., Squires, K.D., 1996. Large eddy simulation of particle-laden turbulent channel flows. Phys. Fluids 8, 1207–1223.

Wang, Q., Squires, K.D., Simonin, O., 1998. Large eddy simulation of turbulent gas–solid flows in a vertical channel and evaluation of second-order models. Int. J. Heat Fluid Flow 19, 505–511.

Yamamoto, Y., Potthoff, M., Tanaka, T., Kajishima, T., Tsujui, T., 2001. Large-eddy simulation of turbulent gas-particle flow in a vertical channel: effect of considering inter-particle collisions. J. Fluid Mech. 442, 303–334.

Zhang, X., Zhou, L., 2004. Simulation of gas-particle channel flows using a two-fluid particle-wall collision model accounting for wall roughness. Paper No. 162, In: 5th International Conference on Multiphase Flow, ICMF '04, Yokohama, Japan, May 30–June 4, 2004.